Available online at www.sciencedirect.com
SCIENCE DIRECT®
Coordination Chemistry Reviews 246 (2003) 229–246
COORDINATION CHEMISTRY REVIEWS
www.elsevier.com/locate/ccr

Doing chemistry on low-dimensional silicon surfaces: silicon nanowires as platforms and templates

Boon K. Teo*

Department of Chemistry, University of Illinois at Chicago, 845 West Taylor Street, 4500 SES, M/C111, Chicago, IL 60607-7061, USA

Received 17 March 2003; accepted 19 June 2003

Contents

Abstract

Silicon-based nanotechnology is highly promising since it is compatible with conventional silicon microtechnology. Recently, there has been considerable interest in the fabrication, characterization, and properties of semiconducting silicon nanowires (SiNWs) and silicon nanodots (SiNDs). SiNWs in the nanosize regime exhibit quantum confinement effects and are expected to play a key role as interconnection and functional components in future nanosized electronic and optical devices. The first-steps towards the fabrication of any devices are the controls of the synthesis and properties of the materials. The purpose of this review is to discuss the surface chemistries of SiNWs and SiNDs in general and the use of these low-dimensional silicon materials as *platforms* and *templates* in creating other nanomaterials in particular. We begin with a brief discussion of the differences in the properties between carbon and silicon, followed by discussions of the synthesis and characterization of SiNWs and SiNDs. We then show how SiNWs can be used as platforms in doing chemistry in the nanorealm, as exemplified by the reductive growths of metal clusters on the surfaces of SiNWs and the formation of metal films on the surfaces of SiNWs. Using SiNWs or SiNDs as templates (molds), a new method for preparing the conventional CNTs or CNOs as well as new nanostructures of hydrocarbon nanotubes (HCNTs) and nanoonions (HCNOs) was discovered. The new HCNTs and HCNOs, with interlayer spacings ranging from 3.5 to 5.9 Å, can be prepared by sonicating SiNWs in common organic solvents under ambient conditions. Two related topics are also discussed. Using zeolites as quasi-templates in the production of SiNWs, ultrafine SiNWs, measuring only a few nanometers in diameter, can be synthesized. Surprisingly, these ultrafine SiNWs exhibit very strong photoluminescence. Using multi-walled carbon nanotubes (MWCNTs) as sacrificial templates, a new type of silicon carbide nanotubes (SiCNTs) can be fabricated. And finally, a

* Tel./fax: +1-312-996-9422.
E-mail address: boonkteo@uic.edu (B.K. Teo).

doi:10.1016/S0010-8545(03)00118-8

brief discussion on the device aspects and other prospects of SiNWs and SiNDs in the future development of Si-based nanotechnology is presented.

Keywords: Silicon nanowires and nanodots; Carbon nanotubes; Platforms; Templates; Low-dimensional materials; Nanomaterials; Surfaces; Synthesis; FTIR; Zeolites; SiC nanotubes; Nanotechnology; Nanodevices; Composites; Coulomb blockade; Single-electron devices

1. Introduction

Nanotechnology [1] is a culmination of many facets of developments in the nanorealm, including nanofabrication, nanomachineries, quantum devices, molecular machines, molecular computers, etc. In principle there are two approaches to this problem: the top–down approach [2,3] and the bottom–up strategy [4]. The first steps in either approach are the synthesis and characterization of nanomaterials and the study of their chemical and physical properties. In fact, nanochemistry allows revolutionary changes of the fundamental properties of materials (often drastically different from those of the bulk phase), giving rise to novel materials and/or new applications.

Low-dimensional nanomaterials, in particular, are of interest in that they may, in addition, exhibit highly anisotropic or dimension-tunable properties, both of which are important attributes in nanodevice applications. Recently, two classes of one-dimensional (1-D) nanomaterials have attracted much attention: carbon nanotubes (CNTs) and silicon nanowires (SiNWs) because of their unique properties. CNTs [5–9] are highly promising low-dimensional nanomaterials because of their highly interesting properties, such as small diameter, high aspect ratio, high mechanical strength, high thermal and chemical stabilities, excellent heat conduction, interesting electrical and electronic properties, etc. [10–21]. In fact, CNTs can be either metallic or semiconducting, with the semiconducting band gap depending upon the tube diameter, geometry, and chirality.

SiNWs are important in nanotechnology because Si-based nanoelectronics is totally compatible with the Si-based microelectronics. SiNWs in the nanosize regime exhibit quantum confinement effects and are expected to play a key role as interconnection and functional components in future nanosized electronic and optical devices [22–37]. It has been suggested that semiconductor wires finer than 100 nm in diameter can be used to develop 1-D quantum-wire high-speed field effect transistors and light-emitting devices with extremely low power consumption [38].

Since carbon and silicon both belong to the same group, it may have suggested that these two elements are similar in their behaviors. In reality, the two elements are very different in terms of their chemical and physical properties. For example, while CNTs are relatively easy to make, the corresponding silicon nanotubes (SiNTs), composed of rolled-up graphite-like sheets, are yet to be synthesized.

While SiNTs are difficult to make, many synthetic routes have been developed in recent years to obtain bulk quantities of SiNWs, using both gas phase and condensed phase techniques [22–26]. A number of interesting properties such as the morphology, structure, photoluminescence, electron field emission, thermal and electronic conductivity and surface chemical property of SiNWs have also been reported [27–37].

The purpose of this review is to discuss the surface chemistries of SiNWs and silicon nanodots (SiNDs) in general and the use of these low-dimensional silicon materials as *platforms* and *templates* in creating other nanomaterials in particular. We shall begin with a brief discussion of the differences in the chemical properties between carbon and silicon (Section 2), followed by a theoretical probe [39] of the reasons behind the stabilities of CNTs and SiNWs (Section 3). In Section 4 we discuss the synthesis and characterization [40] of SiNWs and SiNDs. In Section 5 we shall see how SiNWs can be used as platforms in doing chemistry in the nanorealm as exemplified by the reductive growths of metal ions and preformed metal clusters [41] on the surfaces of SiNWs and the formation of metal films [42] on the surfaces of SiNWs and SiNDs. The former is of interest in that the fabrication of zero-dimensional metallic nanoparticles, which may be considered as “nanodots,” on 1-D semiconducting nanowires (SiNWs) may eventually lead to new nanomaterials or prototype nanodevices. The latter relates to the electrical conductivity of, and patterning of electrical (ohmic) contacts to, SiNWs, both are major issues in the potential applications of SiNWs in interconnection and as basic components for future mesoscopic electronic and optoelectronic devices. In Section 6 we describe a new method in preparing CNTs and a new type of hydrocarbon nanotubes (HCNTs) via sonochemical reactions between SiNWs and common organic solvents [43]. Here the SiNWs or SiNDs serve not only as platforms for the heterogeneous reactions, but also as templates or molds. Two related topics are also discussed. In an attempt to use zeolites as templates in the production of SiNWs, very fine SiNWs, with only a few nanometers in diameter were synthesized (Section 7) [44]. In Section 8 we discuss the use of multi-walled carbon nanotubes (MWCNTs) as templates in the synthesis of silicon carbide nanotubes (SiCNTs) [45], a novel nanostructure for silicon carbide (SiC). And finally, in Section 9, a brief discussion of the device aspects and other prospects of SiNWs and SiNDs in the future development of Si-based nanotechnology will be presented.

2. Si versus C: what are the differences

Carbon and silicon are the two most important elements in the Periodic Table for obvious reasons. They occupy the central stage of the early rows of the Periodic Table by being the first and the second members of Group IV. It is ironic, however, that factors which make carbon unique in nature are also the factors which differentiate these two elements. We shall first describe six important factors (of relevance to the discussions in this review) that distinguish carbon from the rest of the elements in the Periodic Table, followed by a discussion of the distinctions between silicon and carbon.

First, being a Group IV member, carbon has four electrons and four valence orbitals. As such, it is capable of forming four two-center two-electron covalent bonds. Second, carbon, being more electronegative than hydrogen (Pauling's electronegativity $\chi = 2.55$ for C and 2.20 for H), the C–H bonds, unequivocally the most important bond in biology, are polarized as $C^{\delta-}$–$H^{\delta+}$ with the partial negative charge residing on the carbon atom. This implies that nucleophilic attacks generally occur at the hydrogens. Third, while C–H bonds are rather strong (with bond energy of 411 kJ mol^{-1}), carbon bonded to more electronegative atoms such as oxygen and halogens are more reactive (C–O and C–X bonds have bond energies of 357.7 and 485, 327.2, 285 kJ mol^{-1} where X = F, Cl, Br, respectively). Fourth, the small atomic size of carbon means efficient π–π overlap and the formation of stable double and triple bonds. The C–C, C=C, and C≡C bond lengths are 1.54, 1.34, and 1.20 Å, respectively. The C–C, C=C, and C≡C bond energies are 345.6, 602, and 835.1 kJ mol^{-1}, respectively. Fifth, the large energy difference between the valence s and p-orbitals means relatively large hybridization energy for carbon which implies that carbon will "activate" one valence p-orbital at a time, as required by the bonding situation, giving rise to sp, sp^2, and sp^3 hybridizations, thereby forming triple, double, and single bonds, respectively. Sixth, since there are no energetically accessible d-orbitals for carbon to expand its coordination (or valence shell), it makes the racemization of chiral carbon centers rather difficult.

Despite the fact that silicon and carbon both have four valence orbitals and four electrons, the two elements have very different properties. Silicon differs from carbon, in terms of five of the six factors discussed above, in the following ways: (1) lower electronegativity; (2) kinetically more reactive; (3) larger atomic radius, and hence larger orbital size; (4) smaller energy difference between the *s* and the p-orbitals, and hence lower hybridization energies; and (5) the availability of energetically low-lying d-orbitals. These factors impact tremendously on the chemical and physical properties of silicon in comparison to carbon. They will be discussed briefly in this section and developed, albeit qualitatively, into bonding principles which will be used to rationalize many experimental observations in latter sections.

The most important distinction between Si and C is the difference in electronegativity (χ). In contrast to carbon, silicon ($\chi = 1.90$) is less electronegative than hydrogen ($\chi = 2.20$), thereby polarizing the Si–H bonds in the opposite sense, i.e. as $Si^{\delta+}$–$H^{\delta-}$ This implies that nucleophilic attacks on silanes usually occur at the silicon centers. Second, Si–H bonds are significantly weaker than C–H bonds as indicated by their respective bond energies (318 kJ mol^{-1} for Si–H vs. 411 kJ mol^{-1} for C–H). Silanes are also much more reactive than the corresponding hydrocarbon analogs due to the greater polarization caused by the larger disparity in the electronegativities of silicon versus its substituents. Indeed, the greatest bond polarization occurs when silicon is bonded to highly electronegative atoms such as oxygen and halogens (X), giving rise to kinetically labile Si–O and Si–X bonds, despite the fact that these latter bonds are very strong (with bond energies of 452 and 565, 381, 310 kJ mol^{-1} for Si–O and Si–X bonds where X = F, Cl, Br, respectively). It is interesting to note the paradox that Si–O and Si–X bonds are thermodynamically stable on the one hand and kinetically reactive on the other, both due to the very same reason of large bond polarization (i.e. with high ionic characters). Third, the larger atomic size of silicon gives rise to longer Si–Si bonds of 2.35 Å and weaker Si–Si bonds with bond energy of 222 kJ mol^{-1}, in comparison to C–C bonds of 1.54 Å with bond energy of 345.6 kJ mol^{-1}. Furthermore, as a result of the poor π–π overlaps for silicon (smaller than those of carbon by roughly an order of magnitude), Si=Si bonds of 2.16 Å, with bond energy of 327 kJ mol^{-1}, are much weaker than C=C bonds of 1.34 Å with bond energy of 602 kJ mol^{-1}. Fourth, the energy difference between the valence s- and p-orbitals for silicon is only half of the corresponding value for carbon (Si ($E_{3p} - E_{3s} = 5.66$ eV) versus C ($E_{2p} - E_{2s} = 10.60$ eV)). As a result, silicon tends to utilize all three of its valence p-orbitals, resulting in sp^3 hybridization, in contrast to carbon which can "activate" one valence p-orbital at a time to give sp, sp^2, and sp^3 hybridizations. Finally, the relatively low-lying d or other virtual oribitals (such as the antibonding σ* oribitals) allow silicon to expand its coordination sphere from four to five or six. While this attribute greatly enriches the chemistry of silicon, it is detrimental to biological systems which rely, among other things, on the stability of chiral centers. In other words, the expansion of coordination spheres, especially in the case of fluxional behavior in solution, can cause racemization of the chiral centers. This may be one of the reasons why nature chose carbon instead of silicon in building the biological world. The energetically accessible d and/or σ* oribitals of silicon also allow backbonding to occur, with electron densities donated from the lone pair(s) of the bonded atom (substituent) back to the silicon virtual orbitals.

3. SiNW versus CNT: why

Since the discovery of the CNTs [5], there has been considerable interest in the synthesis, structures and electronic

properties of these and other carbon nanostructures, both experimentally [6,7] and theoretically [8,9]. Unlike CNTs, the analogous Si nanotubes, based on rolled-up graphite-like sheets, are yet to be made, though several theoretical investigations have appeared [46–48]. (It should be noted that a new type of silicon nanostructure, described as crystalline silicon nanotubes (cSiNTs), has recently been prepared [49,50]. These nanostructures, however, may also be considered as hollow crystalline SiNWs or nanorods).

In a recent publication [39], we compared the electronic structures of four systems: a diamond-structured carbon nanowire (CNW), a SiNW, a CNT, and a SiNT in order to elucidate the differences in the structures and bonding between cubic (diamond-like) and tubular nanostructures of carbon and silicon with the hope of understanding the reason(s) for the hitherto unsuccessful synthesis of the silicon analogs of the CNTs.

Fig. 1 shows the four model compounds studied in this work. They represent a diamond nanowire, $C_{54}H_{60}$ (**1**), a SiNW, $Si_{54}H_{60}$ (**2**), a CNT, $C_{54}H_{12}$ (**3**), and a SiNT, $Si_{54}H_{12}$ (**4**). The CNT selected here has an armchair (3,3) structure. It is one of the smallest CNTs reported recently [51–53]. Hydrogen atoms were added to saturate the dangling bonds. PM3 parametrization [54] of the MNDO semiempirical hamiltonian [55] was used. The results were further confirmed by ab initio calculations.

For the geometrically optimized nanostructures **1**–**4**, there are general trends of bond length variations. As indicated in Fig. 1, the C–C bonds in structure **1** are about 1.54 Å, as expected for single bonds. Similarly, the Si–Si bonds in structure **2** average about 2.35 Å expected for single bonds. In the CNT **3**, the C–C bond lengths alternate between 1.40 and 1.46 Å, indicating a relatively small degree of C=C versus C–C bond localization. In other words, the small bond length alternation of about 0.06 Å signifies that π delocalization is extensive in CNTs. SiNT such as **4** also shows similar bond length alternation (see Fig. 1), but with a much larger variation of 0.40 Å. The shortest Si–Si bond length is only about 1.85 Å, while the longest is about 2.25 Å, showing a stronger tendency for bond localization (Si=Si vs. Si–Si). As can be seen from Fig. 1, the CNT **3** has a smooth surface and a more-or-less uniform tube diameter. In contrast, the SiNT **4** has a puckered (corrugated) surface and a periodically varying diameter. Furthermore, the ends of SiNT **4** are distorted to form 12 four-membered rings and terminated by H atoms. As a result, both ends of the SiNT **4** are capped with planar hexagonal rings rather than open-ended as in the CNT **3**.

A detailed analysis of the total density of states revealed that tubular structures for silicon are, in general, less stable and tend to relax to the diamond-like structure with tetrahedral configuration, which allows for the largest extent of overlap of the sp^3 hybridized orbitals. The results also suggest that SiNTs are much less stable than the corresponding CNTs; the cause of which can be traced to the differences in the energetics and overlaps of the valence s- and p-orbitals

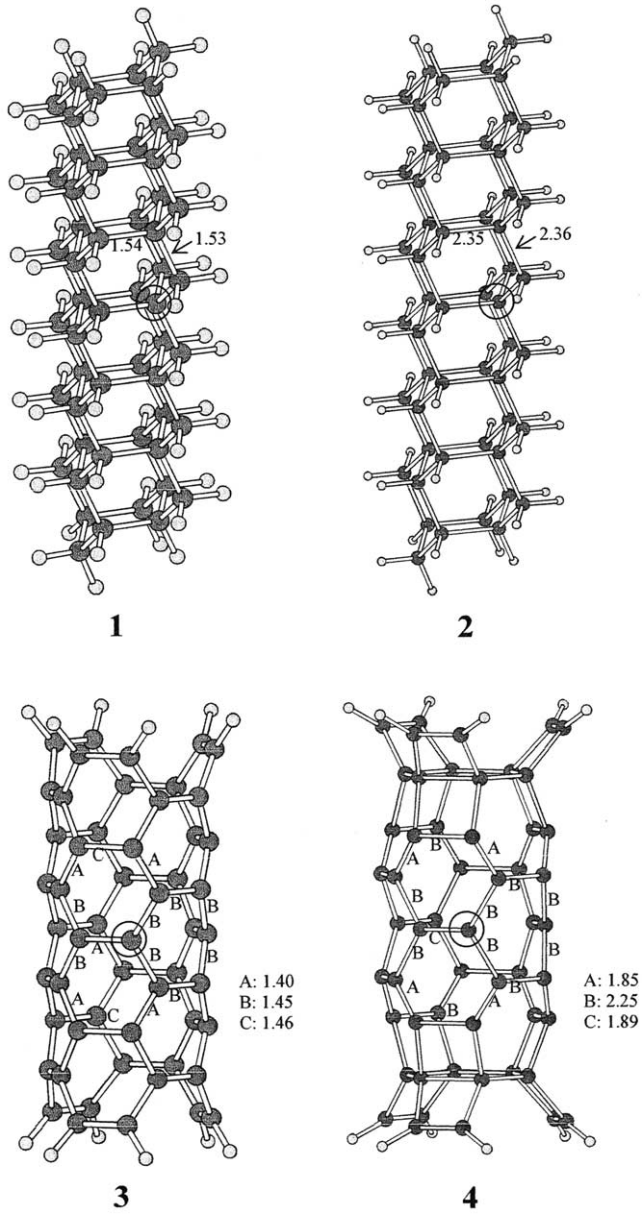

Fig. 1. Four model compounds: a diamond nanowire $C_{54}H_{60}$ (**1**), a SiNW $Si_{54}H_{60}$ (**2**), a CNT $C_{54}H_{12}$ (**3**), and a SiNT $Si_{54}H_{12}$ (**4**). (Reprinted with permission from Ref. [39]. Copyright (2002) Elsevier, B.V.)

of C versus Si discussed in Section 2. In particular, the poor π–π overlap of silicon weakens the π delocalization and under appropriate conditions, may lead to a puckered tubular structure as exemplified by the armchair structure **4**.

4. SiNWs and SiNDs: synthesis and characterization

4.1. Synthesis of SiNWs and SiNDs

Many successful synthetic strategies have been developed to obtain bulk quantities of SiNWs and SiNDs, using both gas phase and condensed phase techniques

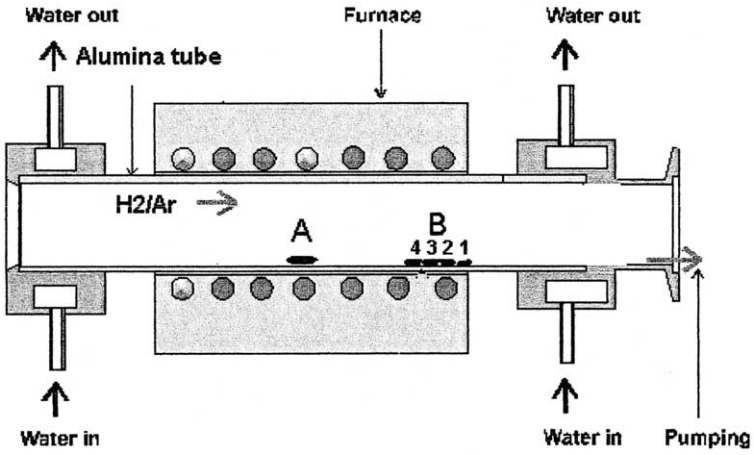

Fig. 2. A schematic diagram of the apparatus used in the synthesis of SiNWs via the thermal evaporation method. (Reprinted with permission from Ref. [45]. Copyright (2002) American Chemical Society.)

[22–26,56–58] with or without metal catalysts. For example, vapor–liquid–solid (VLS) reaction has been used to grow SiNWs of different diameters with metal-catalysts of different sizes [23]. Other growth methods strategies include the oxide-assisted growth (without metal catalysts) via thermal evaporation of silicon suboxide [22–27,56–58]. Since the experimental results discussed in this review were obtained with SiNWs and SiNDs prepared with the thermal evaporation method, we shall describe this technique in some detail.

The equipment used for the thermal evaporation method in the synthesis of SiNWs is depicted schematically in Fig. 2 [45]. An alumina tube was mounted inside a tube furnace. The SiO powders were placed at position A, the middle of the high-temperature zone of the furnace. Silicon wafer or other substrates can be placed at positions marked B1–B4. The tube was evacuated to a base pressure of 10^{-2} Torr. A carrier gas of argon mixed with 5% H_2 was introduced at one end of the alumina tube flowing at 50 standard cubic centimeters per minute (sccm) and at a pressure of 500 Torr. The temperature of the furnace was increased to 1250 °C and kept at this temperature for 40 min. The temperatures at the substrate positions B4, B3, B2, B1 were found to decrease from 980 to 850 °C on the basis of a calibration curve. The products, collected at positions B1–B4 were examined by scanning and transmission electron microscopies.

As noted in the literature [30,26], the SiNWs prepared by thermal evaporation technique are known to have a relatively thick oxide layer. Its presence has been associated with the preferred linear growth of the SiNWs. SiNWs prepared by this method are literally very long (microns), freestanding wires with a diameter of several nm to tens of nm. Each wire has a crystalline silicon core of ca. 15 nm in diameter and is coated with an oxide layer whose thickness is of 1/4–1/3 of the nominal diameter. The majority of the SiNWs grow along the (110) or (112) directions.

4.2. FTIR characterization

The surface properties of bulk Si materials such as Si wafer have been studied extensively for obvious reasons. The most widely used technique for removing silicon oxide from the silicon surface is by etching with dilute hydrofluoric acid. After HF treatment, the silicon surfaces are known to be hydrogen-passivated. During the last decade there have been numerous studies on hydrogen-terminated Si surfaces of bulk silicon materials [59–75]. SiH, SiH_2, and SiH_3 species have been observed on the HF-treated surfaces of Si by high-resolution electron energy loss spectroscopy (HREELS) [59,60], infrared spectroscopy (IRS) [61–70], scanning tunneling microscopy (STM) [71–73], low energy electron diffraction (LEED) [74,75], etc.

As discussed in the previous subsection, the silicon oxide layer of the as-prepared SiNWs or SiNDs serves as a protective layer, rendering the as-prepared SiNWs relatively inert. The inertness of the as-prepared SiNWs is unfavorable for applications of SiNWs in nanotechnology. Further fabrication and/or processing require removal of the oxide layer. It is thus of importance to investigate the surface properties and the stabilities of SiNWs after removal of the oxide layer by HF-etching.

In Ref. [40], attenuated total reflection (ATR) Fourier-transform infrared spectroscopy (FTIR) was used to characterize the surface species on oxide-free SiNWs after etching with aqueous HF solution. Fig. 3 shows the ATR-FTIR spectra in the range of 700–4000 cm^{-1} obtained from, (a) as-prepared SiNWs and; (b) HF-etched SiNWs. In the spectrum of as-prepared SiNWs (Fig. 3(a)), only Si–O vibrations at ∼1050 and ∼800 cm^{-1} were observed. The strong absorption near 1050 cm^{-1} is due to the in-plane stretching vibration involving the Si–O–Si moiety. The absorption at about 800 cm^{-1} is due to in-plane bending vibration involving the same moiety. Upon etching with a dilute (5%) aqueous HF solution, new absorption bands

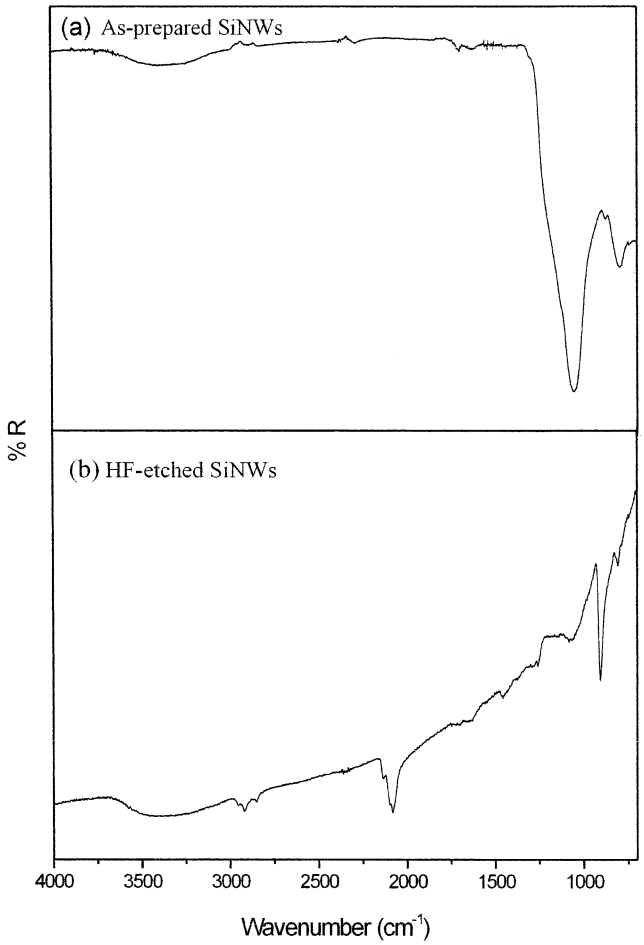

Fig. 3. ATR-FTIR spectra of (a) as-prepared SiNWs and (b) HF-etched SiNWs in the range of 700–4000 cm^{-1}. (Reprinted with permission from Ref. [40]. Copyright (2003) American Chemical Society.)

attributable to Si–H_x (2000–2200 and ~900 cm^{-1}) and CH_x (2800–3000 cm^{-1} due to organic impurities) were observed in the spectrum, while the Si–O absorption bands virtually disappeared (Fig. 3(b)).

Fig. 4 shows the vibrational spectra of HF-etched SiNWs in the frequency range of the Si–H stretching vibrations. Three broad overlapping bands, labeled as M, D and T, can be observed. In accordance with the FTIR results of Si(111) and Si(100) wafers [61–65], the M, D, and T bands were assigned to the monohydride (SiH), the dihydride (SiH_2), and the trihydride (SiH_3), respectively. As is evident from the Fig. 4, these bands are composed of several unresolved peaks due to different chemical adstructures. Detailed assignments of these peaks, labeled M1, M2, M3, D1, D2 and T (also three or more unresolved peaks), can be found in the literature [40,61–65].

In order to specify the adstructures, it is necessary to differentiate between isolated versus interacting vibrational modes of silicon hydrides in the IR spectra. This was accomplished by a deuterated experiment described in Ref. [40]. Suffice it to say here that the shapes of the envelopes of the

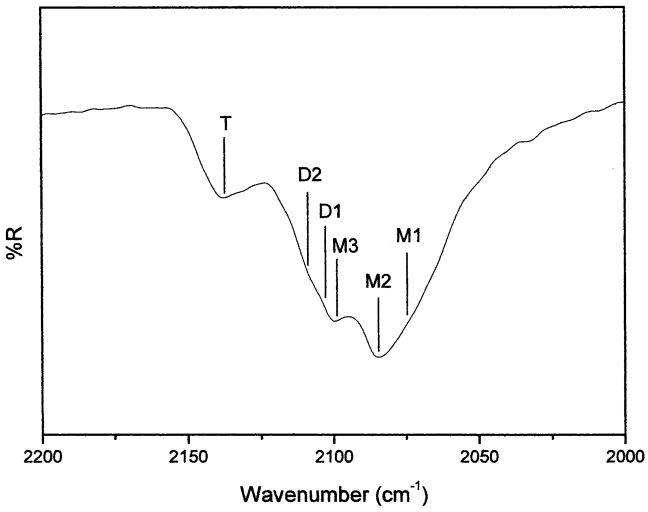

Fig. 4. ATR-FTIR spectrum of HF-etched SiNWs in the range of 2000–2200 cm^{-1}. The expanded Si–H stretching region of Fig. 1(b). (Reprinted with permission from Ref. [40]. Copyright (2003) American Chemical Society.)

SiH_x and the SiD_x peaks are rather similar and the ratios of the Si–H: Si–D stretching frequencies average about 1.38 which agrees with the expected ratio of $\sqrt{2} = 1.41$ on the basis of the mass ratio of 2:1 for D versus H.

The thermal stability of the hydrogen-passivated surfaces of SiNWs was investigated by measuring the FTIR spectra after annealing (in a UHV chamber) at different elevated temperatures. It was found that hydrogen desorption due to the trihydrides occurred at ~550 K and that due to the dihydrides occurred at ~650 K. At or above 750 K, all silicon hydride species began to desorb from the surfaces of SiNWs. At around 850 K, the SiNW surfaces were free of silicon hydride species.

The stabilities/reactivities of HF-etched SiNWs in air and in water were also studied. Hydrogen-passivated surfaces of SiNWs showed good stability in air (under ambient conditions) but relatively poor stability in water [40]. The difference in the stabilities of hydrogen-passivated SiNWs in air versus in water may be associated with the hydroxide ion (albeit very low concentration in neutral solutions) in water, since it is known that hydroxide ions can attack the silicon surface.

We shall end this discussion by summarizing the general characteristics of the reactions between HF and silicon/silicon dioxide. First, despite its behavior as a weak acid, HF is quite reactive, allowing it to etch away the oxide layer. Second, in spite of the extraordinarily strong Si–F bond, the highly polarized Si–F can be kinetically very reactive under ionic conditions, thereby giving rise to H-terminated rather than F-terminated silicon surfaces. And finally, although silicon generally forms covalent bonds (with ionic character), it usually undergoes ionic reactions and/or participates in bimolecular reactions in which bond forming and bond breaking occur simultaneously.

5. SiNW as platforms

5.1. Reductive growths of metal nanodots on the surfaces of SiNWs

The first steps towards building a nanodevice are the synthesis and characterization of nanomaterials and the study of their chemical and physical properties. In this regard, the nanosized polyicosahedral metal (PIMs) clusters [76,77] of well-defined sizes and shapes synthesized and characterized in our laboratory may potentially serve as building blocks for such nanodevices. The metal frameworks of these nanosized Au–Ag clusters can be described as vertex-sharing polyicosahedra. We refer to these high-nuclearity mixed-metal clusters as "clusters of clusters". This "cluster of clusters" growth pathway follows a well-defined growth sequence, from a single icosahedron with 13 atoms ($s_1(13)$) to an icosahedron of 13 icosahedra with 127 atoms ($s_{13}(127)$). The early members of the vertex-sharing polyicosahedral mixed-metal clusters are portrayed in Scheme 1. These ligand-protected nanosized metal particles are of interest in that they exhibit quantum-size effects with properties highly dependent upon the size, shape, structure, and composition of the metal core [76,77]. In an attempt to combine these nanoclusters, which may be considered as zero-dimensional "nanodots," with 1-D semiconducting "nanowires", the heterogeneous reaction between these ligated metal clusters and HF-etched SiNWs was studied. As reported in Ref. [41], the heterogeneous reduction causes a progressive growth of the metal clusters, in a way similar to the homogeneous reductive cluster growth observed in solution [76,77]. In the latter case, progressive reductive condensation of the metal clusters caused by chemical reducing agent [R] is a spontaneous but stepwise agglomeration process of a smaller cluster building block (in this case, an icosahedral cluster unit) as follows (cf. Scheme 1):

$$M^+ \xrightarrow{[R]} s_1(13) \xrightarrow{[R]} s_2(25) \xrightarrow{[R]} s_3(36) \xrightarrow{[R]} s_4(46) \xrightarrow{[R]} \cdots$$

Here M^+ denotes monocationic Au(I) or Ag(I) complexes and [R] represents reducing agents such as $NaBH_4$. In this process, instead of adding one atom at a time, the cluster "grows" by adding one icosahedron at a time, giving rise to the vertex-sharing polyicosahedral growth sequence via spontaneous self-assembly.

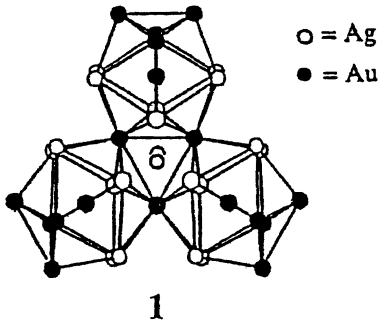

1

Scheme 2.

In Ref. [41], we reported that reductive cluster growth of a triicosahedral cluster, $(Ph_3P)_{12}Au_{18}Ag_{20}Cl_{14}$ (**1**), depicted in Scheme 2, can occur on the surface of the hydrogen-passivated SiNWs. Cluster **1** is a vertex-sharing triicosahedral cluster with 18 gold and 20 silver atoms, encapsulated within a ligand shell containing 12 Ph_3P ligands and 14 chloride ligands. The metal core measures $1 \times 1.5 \times 1.5$ nm^3 and has an oblate shape. The heterogeneous reaction was followed by high resolution transmission electron microscopy (HRTEM).

The TEM images of the products from the reaction of the HF-etched SiNWs with a solution containing cluster **1** are shown in Fig. 5. It was found that the original cluster **1** was reduced to clusters of larger sizes by the SiNWs within minutes. Concomitantly surface Si atoms were re-oxidized to silicon oxide. Based on the time sequence of the HRTEM images, the following general observations can be made. At the beginning, the metal clusters were chemisorbed (anchored) to the SiNW surface (Fig. 5(a)). As the reaction progressed, the anchored metal clusters were reduced by the SiH_x (where $x = 1, 2, 3$) and/or Si atoms on the SiNW surfaces and grew to form larger clusters on the SiNW surface. After about 30 min, metal clusters of different sizes, ranging from 1 to 7 nm in diameter, were observed on the SiNW surface (Fig. 5(b)). In solution, larger metal clusters of 7–25 nm in diameter, as indicated by TEM, were obtained. Metal

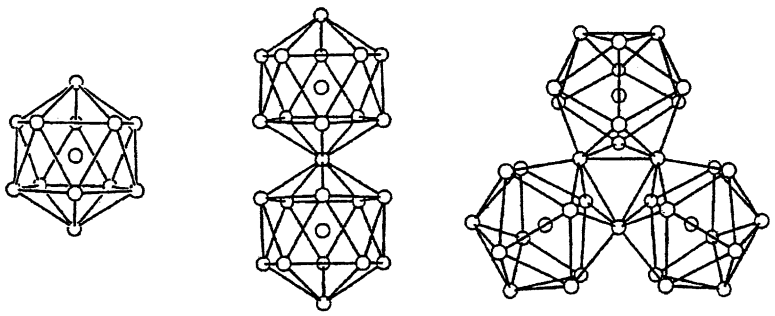

Scheme 1.

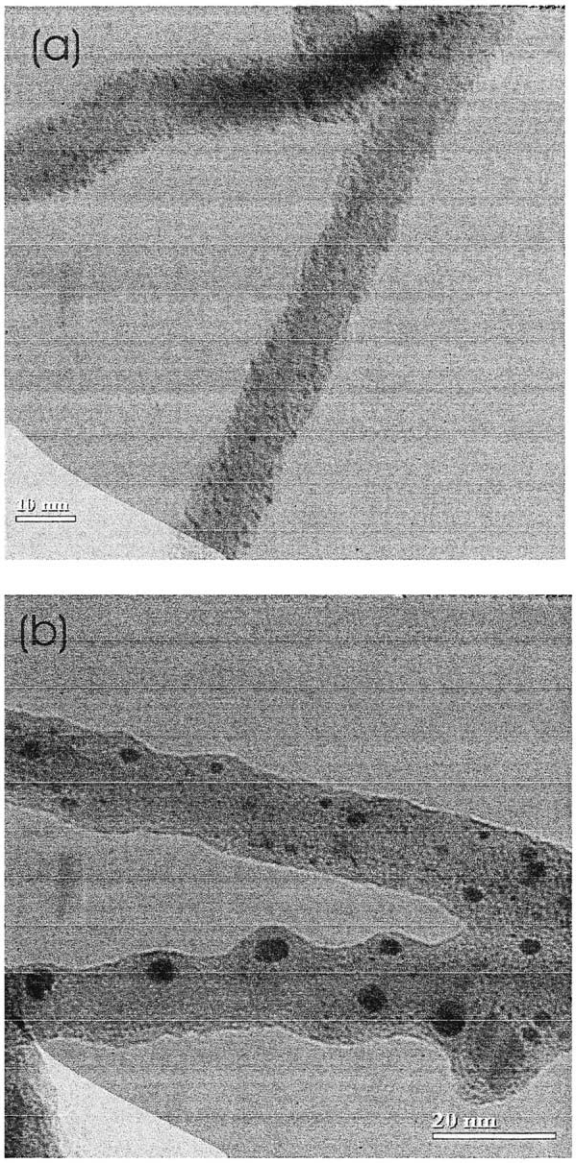

Fig. 5. TEM images of reduced cluster **1** on silicon nanowires: (a) at the beginning of the reaction; (b) after about 30 min. (Reprinted with permission from Ref. [41]. Copyright (2002) American Chemical Society.)

particles of sizes greater than about 5 nm in diameter are bulk-like with the face-centered cubic structure (fcc), as indicated by electron diffraction (not shown). As the metal clusters grew to larger particle sizes (ca. 7–25 nm in diameter), they tended to separate from the SiNW surfaces. And finally, after about an hour, aggregates of these colloidal particles were formed and precipitated from the solution. As a result, the color of the solution turned from dark cherry red at the beginning to light red in about 30 min, and eventually to almost colorless after about an hour. A plausible mechanism for the heterogeneous reductive cluster growth of the Au–Ag cluster **1** on the surfaces of SiNWs can be found in Ref. [41].

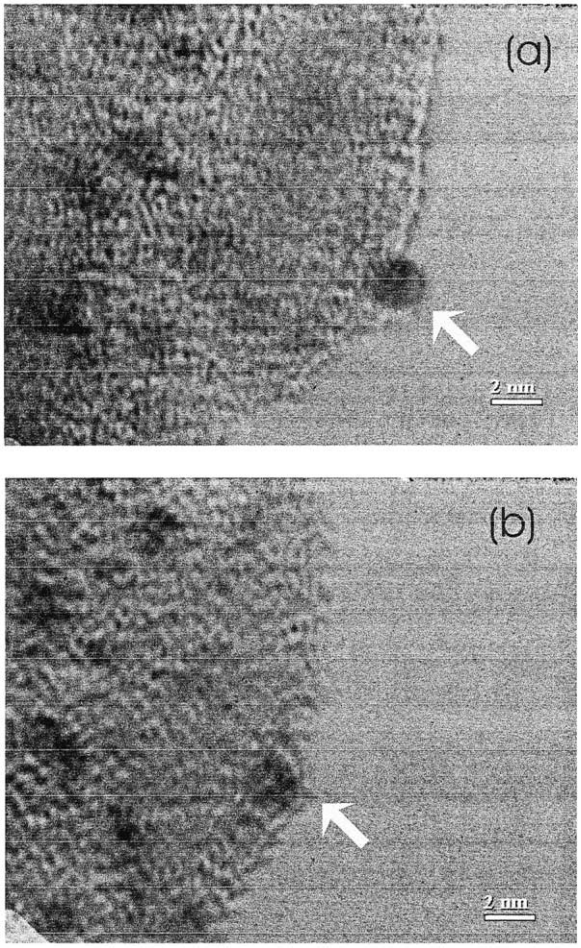

Fig. 6. TEM image of the "sinking cluster" process: (a) in the beginning of the TEM observation; (b) after one minute of TEM observation. (Reprinted with permission from Ref. [41]. Copyright (2002) American Chemical Society.)

Two interesting phenomena, the "sinking cluster" and the "cluster fusion" processes, were observed during the TEM observation of the reaction products. It was found that some metal clusters attached on the SiNW surface were sinking into the amorphous oxide layer under TEM observation. This observation may be likened to a cluster "sinking" in a "sea" of oxide layer. Two snap shots of the entire process are depicted in Fig. 6. In the beginning of the TEM probe, the cluster of ca. 2 nm in diameter (indicated by an arrow in Fig. 6(a)) on the surface kept on throbbling under the intense electron beam of TEM (while barely attached to the SiNW). Eventually the cluster began to sink beneath the surface of the oxide layer. And, after about 1 min, it was completely submersed in the oxide layer (Fig. 6(b)). Similar phenomenon was also observed by Marks et al. [78,79], when the same ligated Au–Ag clusters were deposited on magnesium oxide and examined by the TEM [79]. We believe that, in both cases, the ligands play a role in the cluster "sinking" process. In other words, under intense electron beam irradiation, some of the phosphine and/or chloride

ligands on the cluster were lost and the cluster became coordinatively unsaturated and hence was unstable. The oxide ions in the silicon oxide layer became the replacement ligands, thereby stabilizing the cluster. Phenomenological the metal cluster "sank" into the oxide layer, some were completely submersed, while others only partially.

Another interesting phenomenon observed here is the "fusion" or "aggregation" of metal clusters (see Fig. 5 of Ref. [41]). It was found that clusters can travel by a distance more than ten times its size. The driving force of the migration of nanoparticles on the substrate surface under TEM observation have been well discussed [80–84]. The electron beam induced effects [80–84] as well as Ostwald ripening [85] (growth of large clusters as a result of dissolution of smaller ones) or coagulation processes had been invoked to explain the phenomenon. Since the rates of both the sinking and the aggregation processes appear to increase with increasing electron fluxes, it was suggested that electron irradiation, rather than thermal effects, provides the driving force for these processes [41].

5.2. Formation of metal films on the surfaces of SiNWs

The potential applications of SiNWs in interconnection and as basic components for future mesoscopic electronic and optoelectronic devices [86] raise the issues of electrical conductivity of SiNWs and the patterning of electrical (ohmic) contacts to SiNWs. Although SiNWs can be

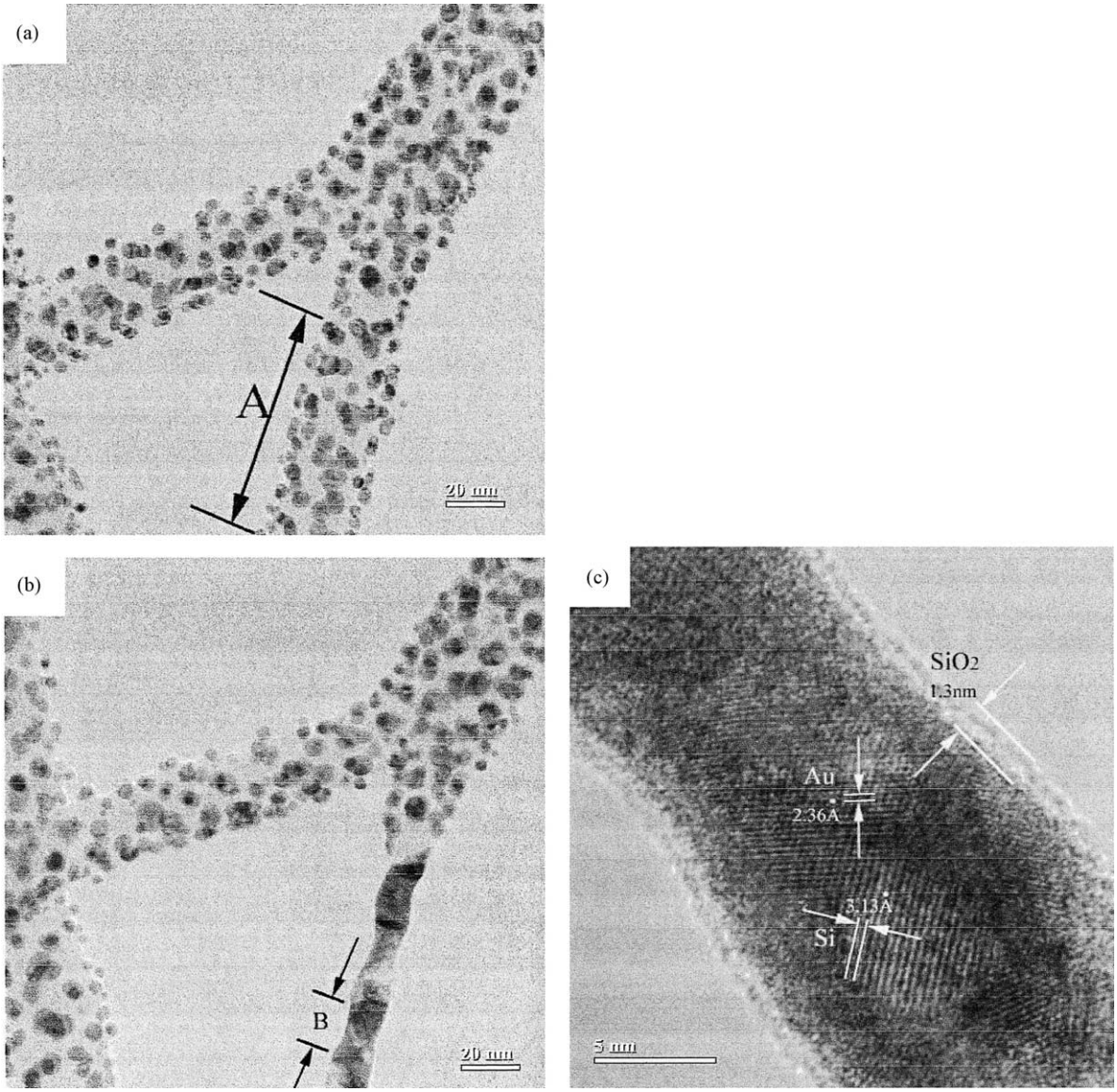

Fig. 7. (a) The Au nanoparticles, with an average diameter of 5 nm, are randomly attached to the surface silicon oxide layer of the SiNWs. (b) The region marked "A" (in (a)) was annealed by the electron beam in the TEM. It can be seen that all Au particles in this region transformed into a metallic layer covering the surface of the SiNW, (c) Corresponding to region "B" in (b), a HREM image shows an Au film covering the SiNW, which is in turn covered by a SiO_2 layer of about 1 nm. (Reprinted with permission from Ref. [42]. Copyright (2002) American Chemical Society.)

mass-produced [87,88], it is difficult to increase the electrical conductivity of SiNWs during the growth process. A number of strategies have been developed in order to provide ohmic contacts to SiNWs, including deposition of Ag particles on SiNWs by chemical methods [34], or formation of metal silicide layers on SiNWs [89]. In a recent paper, [42] we reported a simple and effective technique to fabricate a metal thin film on the surface of SiNWs.

In Fig. 7(a), the Au nanoparticles, with an average diameter of 5 nm, were deposited onto the silicon oxide surfaces of the SiNWs via argon-ion sputtering. Most, if not all, of the Au particles were crystalline with distinct facets. Some of the Au nanoparticles, however, aggregated to form larger fused clusters. The region marked "A" was annealed by the electron beam in the TEM. It can be seen that all Au particles in this region were transformed into a metallic layer covering the surface of the SiNW as depicted in Fig. 7(b). The diameter of the annealed region was reduced about 50% in comparison with the original oxide-covered SiNWs. Corresponding to region "B" in Fig. 7(b), a HRTEM image shows an Au film covering the SiNW which is in turn covered by a SiO_2 layer of about 1 nm, as shown in Fig. 7(c). Judging from the lattice parameters (d spacings), the Au film and some bared (uncovered) Si spots can be found on the SiNW surfaces as shown in Fig. 7(c).

Fig. 8(a–d) depict the snapshots and the time sequence of the Au film formation process. In Fig. 8(a), a polyhedral Au nanoparticle, about 5 nm in diameter, was attached to the surface of a SiNW. Part of this Au nanoparticle was covered by SiO_2 (serving as ligands). In Fig. 8(b), the attached SiO_2 ligand began to disappear, and the Au nanoparticle started to sink into the SiO_2 layer of SiNW. In Fig. 8(c), half of the Au nanoparticle merged with the existing Au film layer. In Fig. 8(d), the entire Au nanoparticle disappeared and integrated with the existing Au film layer. It is interesting to note that, in the process (Fig. 8(b–d)), the Au nanocrystal rotated and reoriented to match the lattice orientation of the existing Au film layer.

In the second part of the study, SiNWs with the oxide layer removed (by HF etching) were coated with Au nanoparticles and annealed by an electron beam in the same fashion. The results are rather similar. The readers are referred to Ref. [42] for details.

A mechanism of the Au film formation by electron-beam annealing is proposed in Fig. 9. The Au nanoparticles were deposited on the SiO_2 layer of the SiNWs as shown in

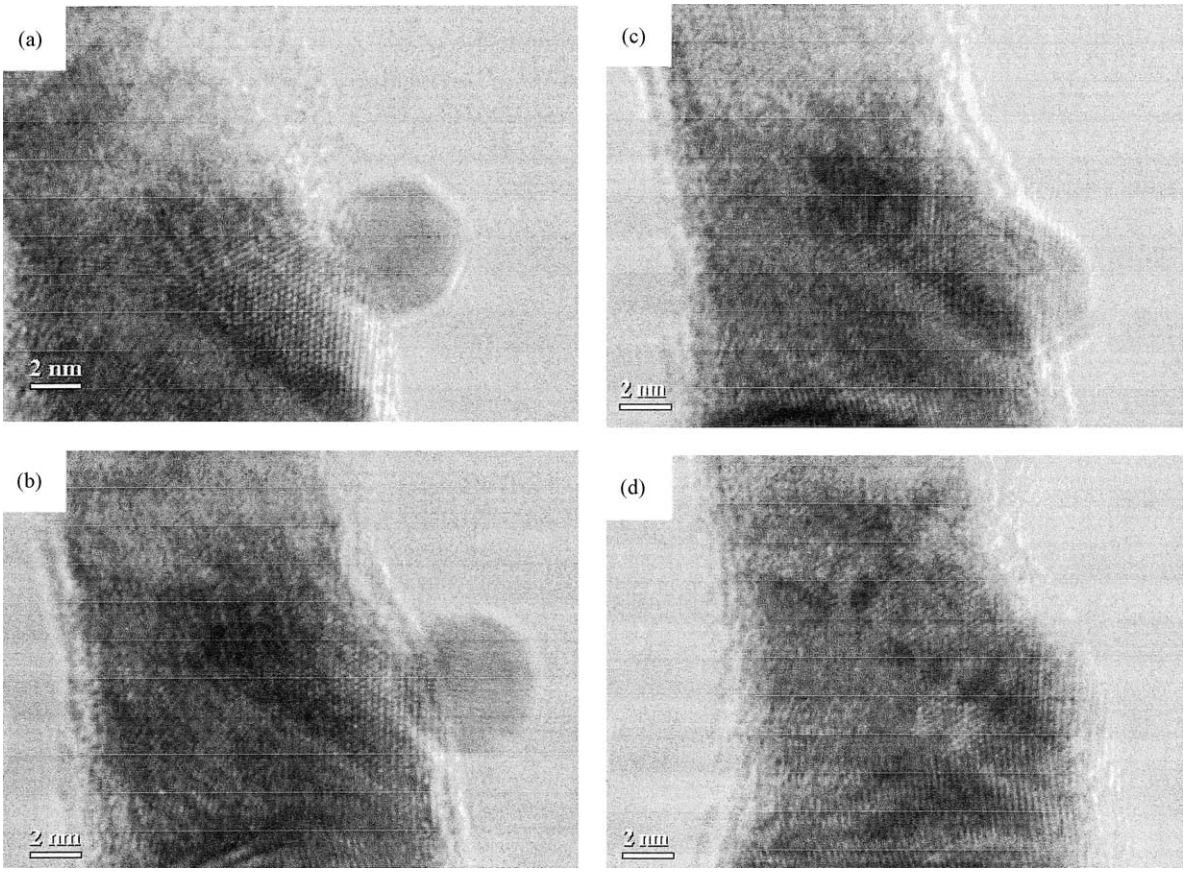

Fig. 8. (a) A polyhedral Au nanoparticle, about 5 nm in diameter, was attached to the surface of a SiNW. (b) The attached SiO_2 ligand began to disappear, and the Au nanoparticle started to sink into the SiO_2 layer of SiNW. (c) Half of the Au nanoparticle merged with the existing Au film layer. (d) The entire Au nanoparticle disappeared and integrated with the existing Au film layer. (Reprinted with permission from Ref. [42]. Copyright (2002) American Chemical Society.)

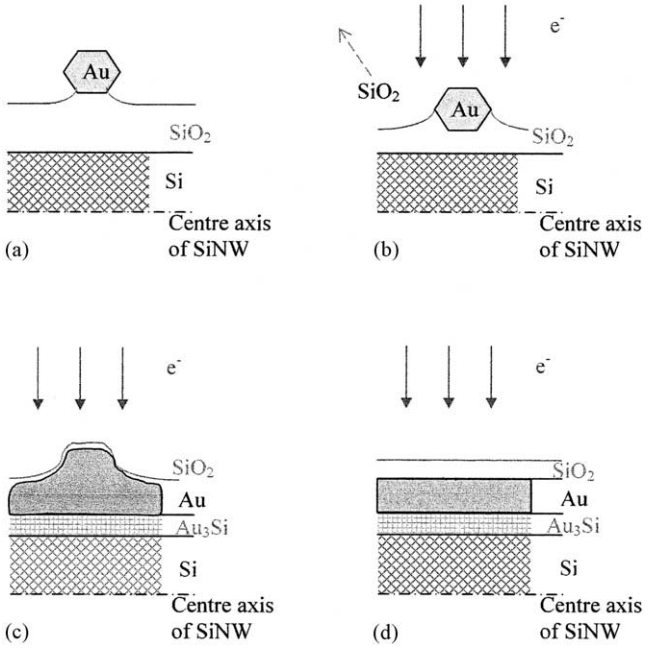

Fig. 9. Proposed mechanism of the Au film formation by annealing under the converging electron beam of TEM. (Reprinted with permission from Ref. [42]. Copyright (2002) American Chemical Society.)

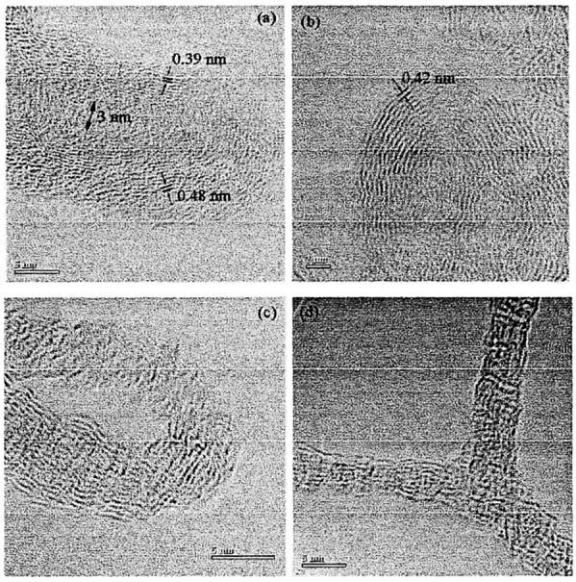

Fig. 10. HRTEM images of a new type of hydrocarbon nanomaterials: (a) nanotube (inner and outer diameters of 3 and 18 nm, respectively), (b) nano onion, (c) loop and (d) Y shape carbon nanostructures with interlayer spacing larger than 3.4 Å. (Reprinted with permission from Ref. [43]. Copyright (2002) American Chemical Society.)

Fig. 9(a). In Fig. 9(b), as this area was exposed to the converging electron beam, some of the SiO_2 were "blown away" by the intense electron beam; some were reduced to silicon by the negatively charged electrons. This explains why the diameter of the SiNWs with oxide layer was reduced by more than 50%. The SiO_2 layer that remained was softened and "wetted" the attached Au nanoparticles. The surface tension provided a driving force that drew the Au nanoparticles into the oxide layer. This is similar to the "sinking cluster" phenomenon described in the previous subsection. In the process, some of the Au nanoparticles aggregated to form larger (fused) clusters, some reacted with Si to form silicides such as Au_3Si (as indicated by electron diffraction) at the interface**,** as shown in Fig. 9(c). And the Au nanoparticle rotated and reoriented to match the lattice of the existing Au film. As the annealing process proceeds (see Fig. 9(d)), the Au nanoparticles continues to integrate into the existing Au lattice to form a continuous Au film. Eventually, the SiNW was covered with an Au_3Si layer, followed by an Au layer, and a thin outermost SiO_2 layer.

The mechanism for the Au film formation for the HF-etched SiNWs is probably the same, except that there is little or no oxide layer to impede the diffusion of Au particles onto the surfaces of the SiNWs.

6. SiNW as templates: syntheses of carbon and hydrocarbon nanostructures

Nowadays, CNTs [5,90] and nanoonions (CNOs) [91] can be synthesized by such diverse techniques as arc discharge [5,92], laser ablation [15], chemical vapor deposition (CVD) [93], electron beam irradiation and high temperature annealing [91,94], etc. Until now, however, these carbon nanostructures can only be produced under such severe conditions as high temperature, high vacuum, high voltage arc discharge or high-energy electron irradiation, though there were recent reports of the syntheses of CNTs [95] and CNOs [96] by arc discharge using graphite electrodes in water at room temperature. Furthermore, many of these preparative methods require specialized equipments such as lasers and CVD or metal catalysts. In a recent paper [43], we reported a simple sonochemical solution method using SiNWs as templates to produce carbon nanotubular structures under ambient conditions (room temperature and atmospheric pressure) and without metal catalysts.

The unexpected discovery grew out of our attempt to disperse oxide-free SiNWs in common solvents. These carbon nanotubular structures can be produced by dispersing HF-etched SiNWs in certain common organic solvents such as $CHCl_3$, CH_2Cl_2, CH_3I, etc., followed by bath sonication for 15 min under ambient conditions. The yellowish solution turned turbid within minutes of sonication and exhibited Tyndal effect characteristic of colloidal solutions.

In addition to the commonly observed CNTs and CNOs (not shown) with interlayer spacing of 3.4 Å, a new type of hydrocarbon (HC) nanostructures, with interlayer spacing varying from 3.5 to 5.8 Å, was observed. These nanostructures exhibit many shapes and forms, the most common ones being multi-walled HCNTs and onions (HCNOs) as depicted in Fig. 10(a and b), respectively. Other shapes such as faceted polyhedral onions, twisted tubes or loops

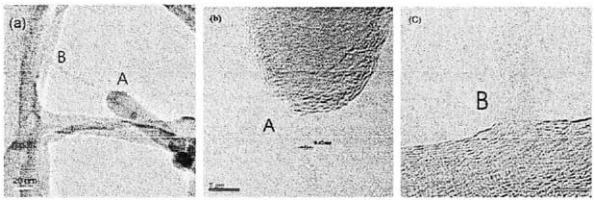

Fig. 11. (a) TEM image of a HCNT connecting the tip of a SiNW (A) to the body of another SiNW (B); (b) HREM image taken from area "A" in (a); (c) HRTEM image taken from area "B" in (a). (Reprinted with permission from Ref. [43]. Copyright (2002) American Chemical Society.)

(Fig. 10(c)), Y-shape (Fig. 10(d)), or other networks of tubes can also be found. These carbon nanostructures are different from conventional CNTs and CNOs in that they all have rough, wavy layers and are easily shrunk, collapsed or damaged by the electron beam under TEM. Nonetheless, these HCNTs/HCNOs exhibit well-structured morphologies and can be converted to the conventional CNTs/CNOs (with interlayer spacings of 3.4 Å) upon prolonged sonication.

We believe the SiNWs serve as templates for the formation of these nanostructrues, as evidenced by the "caught-in-the-act" TEM picture shown in Fig. 11(a). Here, a HCNT of about 4 nm in diameter and 65 nm in length was found to connect the tip of one SiNW (A) to the body of another SiNW (B). The SiNWs have diameters of about 30 nm. The EELS results, taken from area between "A" and "B", reveal that it comprises purely of carbon. Fig. 11(a) may also be described as a nanoscaled "SiNW in a CNT".

The HRTEM image in Fig. 11(b), taken from area "A" in Fig. 11(a), shows that this particular HCNT has an interlayer spacing of 4.2 Å, emanating from the tip of SiNW A. This seven-layered HCNT (or a total of 14 layers) is connected to SiNW B as shown in Fig. 11(c), taken from area "B" in Fig. 11(a). TEM element mapping results (not shown) also confirmed the chemical compositions of the SiNW (the template) and the HCNT (the product).

It is believed that the new carbon structures are associated with active reaction sites on the surfaces of the SiNWs. In this respect, when the as-synthesized SiNWs (sheathed with an oxide layer) were immersed in $CHCl_3$ and treated by bath sonication in the same way, no carbon nanostructures were found. This result confirmed that the carbon nanostructures arose from the reactions between the $–SiH_x$ ($x = 1$, 2, 3) species on the surfaces of the SiNWs and the solvent molecules. These findings provide a clue to the mechanism of formation of the HCNT(O)s/CNT(O)s. On the surfaces of the SiNWs, the organic solvent molecules react with the SiH_x moieties, and, under the local heating condition of the sonication process, result in the elimination of the substituents of the solvent molecules. In the case of $CHCl_3$, the reaction between the Si–H and C–Cl bonds results in dehydrochorination of the $CHCl_3$ molecules, giving rise to CH units which polymerize to form the hydrogenated graphite sheets [97] that wrap around the SiNWs (templating effect). Further sonication causes the SiNWs to shed off the HCNTs, refreshing the SiNW surfaces for further reaction. The extruded HCNTs or HCNOs usually collapse to form solid or hollow tubes or onions of smaller diameters (see Fig. 10). A solid HCNT extruded from a SiNW is depicted in Fig. 11(a). And finally, these hydrocarbon nanostructures may ultimately transform (sometimes partially) to the conventional CNTs and CNOs with interlayer spacings of 3.4 Å upon prolonged sonication, resulting in hybrid HCNT(O)s/CNT(O)s, and, ultimately, to CNT(O)s.

We believe that these new structures of HCNTs/HCNOs are formed by networks of chair-form cyclohexane-like hexagonal structure, similar to that of partially hydrogenated graphite on the one extreme and that of the amorphous hydrocarbon (a-C:H) on the other. Morphologically, they are similar to the conventional CNTs or CNOs except that C–H bonds have been inserted between layers, thereby converting curved sp^2 sheets into puckered sp^3 layers or combinations thereof. The more C–H bonds being inserted, the larger will be the interlayer spacing. The interlayer spacing also depends on the degree of packing between adjacent layers. The single-tube EELS of a HCNT is compared with that of a conventional CNT in Fig. 12. The main difference between the new HCNT and the conventional CNT is that HCNT exhibits less sp^2 bonds and more disordered sp^3 bonds than does CNT, as evidenced by the fact that the edge ratio sp^3 (C–C)/sp^2 (C=C) is ca. 1 for the conventional CNT but 1.5 for the new HCNT.

The Raman spectra of the products further confirmed the carbon structures are the reaction products of SiNWs and the solvent molecules. The intense peaks at 517 and 960 cm^{-1} can be ascribed to the scattering of the first-order optical phonon and the overtone of TO (L) of Si in SiNWs, respectively. More importantly, there were three weak peaks at 1300, 1450, and 1600 cm^{-1}. The peaks at 1300 and 1450 cm^{-1} can be assigned to sp^3 (C–C) whereas that at 1600 cm^{-1} to sp^2 (C=C) stretching frequencies of the HCNT(O)s. These bands are very different from that of normal CNTs

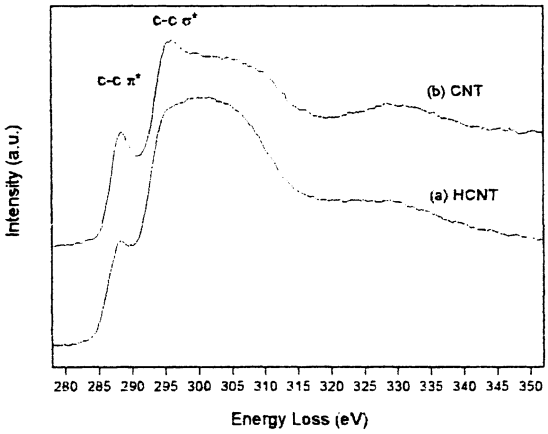

Fig. 12. The single-tube EELS results of the new HCNT (curve a) and the conventional CNT (curve b). Both were found in the same sample. (Reprinted with permission from Ref. [43]. Copyright (2002) American Chemical Society.)

which has a strong band at 1580 cm^{-1} (sp^2) and a weaker band at 1348 cm^{-1} (sp^3).

In summary, both the conventional CNTs and nanoonions (with interlayer spacings of 3.4 Å) and the new HCNTs and nanoonions (with interlayer spacings ranging from 3.5 to 5.9 Å) can be prepared by reacting SiNWs with common organic solvents in a laboratory sonicator under ambient conditions. It is believed that sonication not only promotes the reaction between SiH_x [40] and the organic molecules but also facilitates the formation of the different types/shapes of carbon nanostructures as well as causes the extrusion (or demolding) of the products. Future work will allow the optimization of the yields of the various types of carbon and hydrocarbon nanostructures.

7. Zeolites as quasi-templates: synthesis of ultrafine SiNWs

The control of the diameter and uniformity of SiNWs is a crucial factor in the design and fabrication of nanoscale devices. In a recent paper [44], we reported a new method for the preparation of very fine (1–5 nm) and uniform SiNWs using zeolites as templates.

Fig. 13 is an overview of the SEM image of the SiNWs. A large quantity of SiNWs was found on the surface of zeolite Y pellets. Most of the SiNWs were attached to the surface of the zeolite pellet. Fig. 14 is the TEM image of a single SiNW. We found that each SiNW has an ultrafine crystalline silicon core and a thick amorphous silicon dioxide outer layer. The diameters of the Si cores range from 1 to 5 nm, with the dominant diameter of 3 nm. These Si cores are very fine and uniform in diameter throughout the entire length (~1 μm or longer) of each wire. The diameter of the amorphous SiO_2 layer of the SiNWs ranges from 20 to 40 nm. In this particular SiNW, a central Si core of 1.3 nm in diameter and a relative thick SiO_2 outer layer of 25 nm in diameter were observed. Assuming a Si–Si bond length

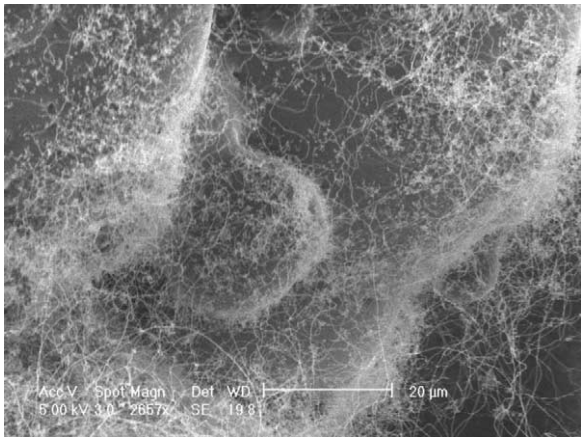

Fig. 13. A typical SEM image of the SiNWs on zeolite Y. (Reprinted with permission from Ref. [44]. Copyright (2002) Elsevier, B.V.)

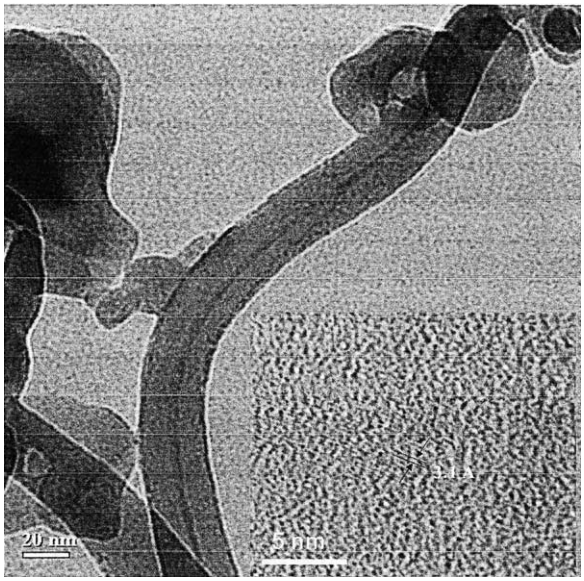

Fig. 14. The TEM image of a typical single SiNW with a Si core diameter of 3 nm covered with a SiO_2 layer of 28 nm. The inset is the HRTEM image of the same SiNW. (Reprinted with permission from Ref. [44]. Copyright (2002) Elsevier, B.V.)

of 0.235 nm, this SiNW of 1.3 nm in diameter contains only six to seven silicon atoms in the lateral dimension. The amorphous oxide surface of this wire is quite rough. The inset of Fig. 14 shows a HRTEM image of the same SiNW. It confirms that the core is crystalline silicon with 3.1 Å d spacing of the (111) planes. To the best of our knowledge, these are the finest SiNWs synthesized (in bulk quantities) to date.

Fig. 15 shows a proposed mechanism for the formation of these very fine and uniform SiNWs. The growth of the SiNWs is similar to the previously described oxide-assisted growth mechanism [22–27,56–58]. The SiO powders were firstly sublimated at 1250 °C and formed nanoclusters in the vapor phase. The SiO nanoclusters subsequently deposited on the surface of zeolites and some diffused into the channels of the zeolites (positioned downstream, at 930 °C) as shown schematically in Fig. 15(a). At this temperature regime, SiO nanoclusters disproportionated to form Si and

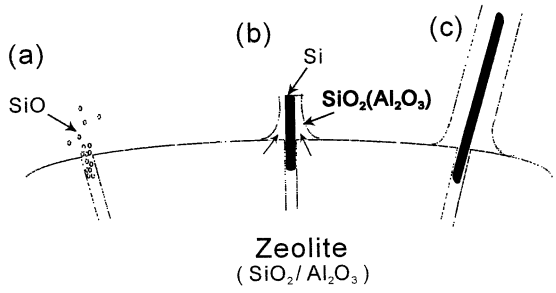

Fig. 15. Proposed growth mechanism for the very fine and uniform SiNWs. (Reprinted with permission from Ref. [44]. Copyright (2002) Elsevier, B.V.)

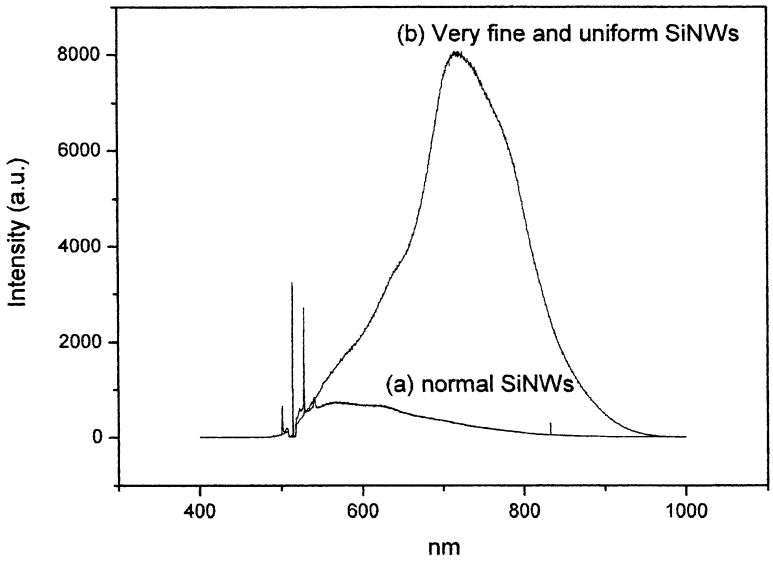

Fig. 16. The photoluminescence spectra from (a) normal SiNWs of 20–50 nm in diameters and (b) ultrafine and uniform SiNWs of 1–5 nm in diameters synthesized with zeolites. (Reprinted with permission from Ref. [45]. Copyright (2002) American Chemical Society.)

SiO_2 and resulted in the precipitation of silicon nanoparticles (the nuclei of Si nanowires) surrounded by shells of silicon oxide. The nucleation process was limited by the openings of the channels and a large quantity of SiO_2 in zeolites limited the lateral growth. As a result, the core of SiNWs was limited to 1–3 nm in diameter at the nucleation stage. At the same time, the zeolite supplied additional silicon oxide to form the shell of the SiNW, resulting in an oxide layer much thicker than normal, as shown in Fig. 15(b). At this point, the "oxide-assisted" growth process became operative, with the "oxide" being primarily supplied "in situ" by the zeolites. Each SiNW seems to have a "root" in the zeolite, as shown schematically in Fig. 15(c).

Surprisingly, as shown in Fig. 16, these ultrafine SiNWs exhibit very strong photoluminescence (which centers at around 720 nm, curve b) in comparison with that of normal SiNWs of about 20 nm in diameter (which peaks at around 600 nm, curve a). It is possible that the strong photoluminescence is related to quantum-size effect, though we cannot rule out the effect due to the "impurity" of aluminum ions (from zeolite) in the silicon oxide layer.

8. CNTs as reactive templates: synthesis of SiCNTs

The discovery of CNTs opens up new and exciting possibilities for making different kinds of nano-sized heterostructures by filling the inside hollow space with other elements or by decorating the outside surfaces of the nanotubes. For example, SiC, [98,99] gallium nitride nanowires [100], Si–B–C–N nanocables [101], heterostructures of CNTs and carbide nanorods [102], and SiC–SiO_x biaxial nanowires [103] have recently been synthesized using CNTs as templates. These fabrication methods using CNTs as templates are highly promising due to the morphological integrity of CNTs which spatially confine the reaction to the nanotubes. The net result is the formation of 1-D products with diameters, lengths, and orientation similar to that of the CNT templates [99].

Among the various semiconducting materials, SiC possesses unique physical and electronic properties which make it a suitable material for the fabrication of electronic devices for high temperature, high power, and high frequency applications [104]. 1-D SiC nanosystems may exhibit unique properties due to quantum-size effects, making them useful materials in nanotechnology and nanoscale engineering.

In Ref. [45], the growth of 1-D nanostructures of SiC was observed in the reaction between silicon (produced by disproportionation of SiO) and CNTs (as templates) in a tube furnace (at about 935 °C). The original intent was to synthesize SiNTs (see Section 3) using CNTs as templates. Instead, several types of interesting SiC nanostructures were obtained. First, silicon carbide nanowires with 2.5 Å spacing of the {111} planes of β-SiC with the cubic zinc blend structure were obtained**.** The result is in accord with the report of Z. Pan et al. [99]. The second nanostructure obtained was the biaxial nanowires of silicon carbide-silicon oxide (see Fig. 3(a and b) of Ref. [45]). A similar biaxial structure had been observed by Wang et al. [103]. The biaxial SiC–SiO_x nanowires consist of two side-by-side subnanowires of β-SiC and silica.

A third type of nanostructure, which may be described as SiCNT, was observed for the first time. A typical image is shown in Fig. 17(a). Element mappings (Fig. 17(b, c)) showed the multi-walled tube structure to be composed of Si and C. Furthermore, the interlayer spacings of these new Si-containing multi-walled nanotubes are significantly larger than those of 3.4 Å normally observed for MWCNT

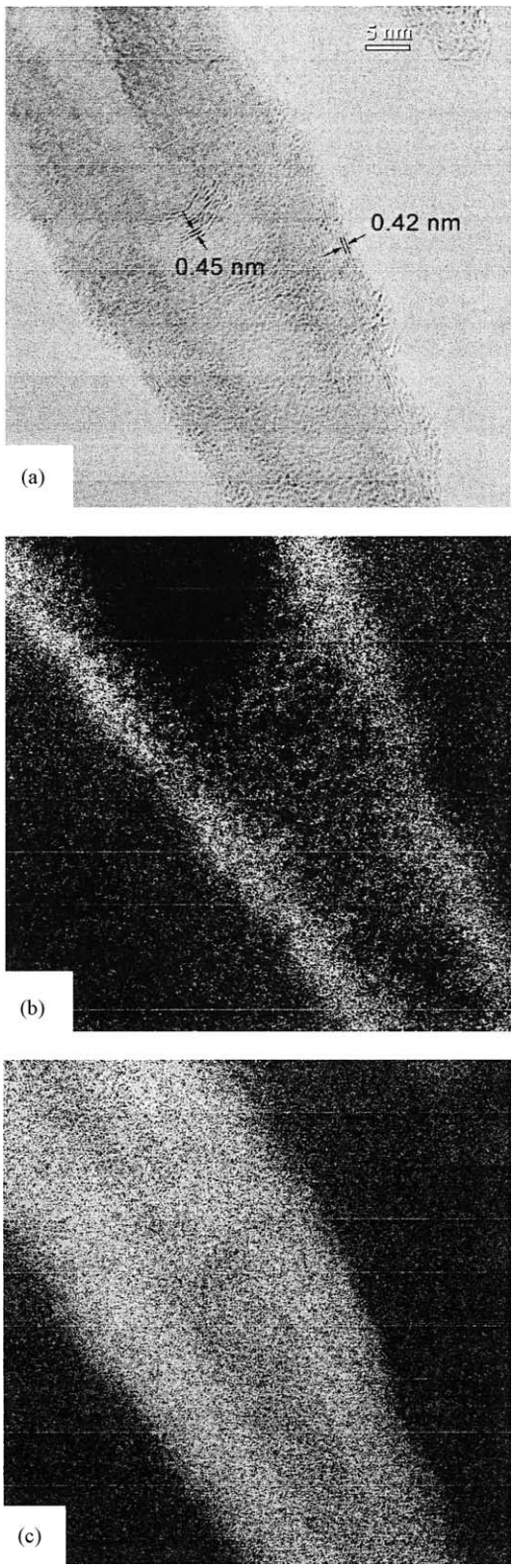

Fig. 17. (a) The HRTEM image of SiC nanotube structure with 4.2 and 4.5 Å interlayer spacings. (b) Si element mapping. (c) C element mapping. (Reprinted with permission from Ref. [45]. Copyright (2002) American Chemical Society.)

(for example, 4.2 and 4.5 Å in Fig. 17(a)). They are best described as multi-walled SiC nanotube (MWSiCNT) grown on a MWCNT (as sacrificial template) [45].

It is known that silicon carbide can form when Si meets C at a sufficiently high temperature (T) (roughly $T > 800\,^{\circ}C$) [102]. At the temperature of about 935 °C, Si and C react to form SiC. The transformation of CNT to a SiCNT is controlled by the diffusion of Si to the SiC | C interface. However, Si diffusion rate through bulk SiC is extremely slow in the temperature range of 800–1000 °C. A continuous supply of Si atoms from the disproportionation of SiO is, therefore, transported primarily via surface diffusion [105]. This is consistent with the observation that the SiC was formed layer by layer via surface diffusion of Si atoms into the MWCNT [45].

The EELS spectrum (curve (a) in Fig. 18) of a single multi-walled SiCNT shows that the Si $L_{3,2}$-edge shifts to a higher energy at 101.2 eV (from 99.3 eV of pure silicon) and the C K-edge shifts to a low energy at 282.5 eV (from 284 eV of pure carbon), indicating a strong chemical bonding between Si and C. This is to be expected based on the fact that carbon is more electronegative than silicon. The EELS of SiCNT is contrasted with the EELS of β-SiC nanowire (curve (b) in Fig. 18). With the exception of the pre-edge peaks, the two EELS spectra are rather similar. The strong pre-edge absorption peaks of both the Si and the C EELS of SiCNT (curve (a) of Fig. 18) are indicative of the π bonding between Si and C (compare with curve (b) of Fig. 18 for β-SiC).

It was concluded that the observed multi-walled SiC nanotube is a new polytype of SiC, with interlayer spacings ranging from 3.5 to 4.5 Å, distinctly different from those of the amorphous SiC or any of the common crystalline SiC phases (such as the cubic (3C), hexagonal (4H, 6H), or rhombohedral (15R) structures, etc.) [104]. It was also proposed that the structure of these new SiC nanotubes is similar to that of CNTs with silicon atoms substituting half of the carbon atoms in the curved hexagonal graphite tube structure.

9. Nanodevices

The anisotropic properties of low-dimensional nanomaterials such as nanowires, nanorods, nanowhiskers, nanotubes, etc. are highly desirable attributes in the design and fabrication of nanodevices. In fact, nanoelectronic devices such as transistors, logic gates, tweezers, sensors, etc. have been built from CNTs [106]. However, the electronic properties of CNTs are highly dependent on the tube diameters and their structures, both of which are difficult to control. By contrast, the diameters, structures, and compositions of nanowires are, relatively speaking, easier to control, making them good candidates for the fabrication of nandevices.

Silicon-based nanotechnology, in particular, is promising since it is totally compatible with the conventional silicon

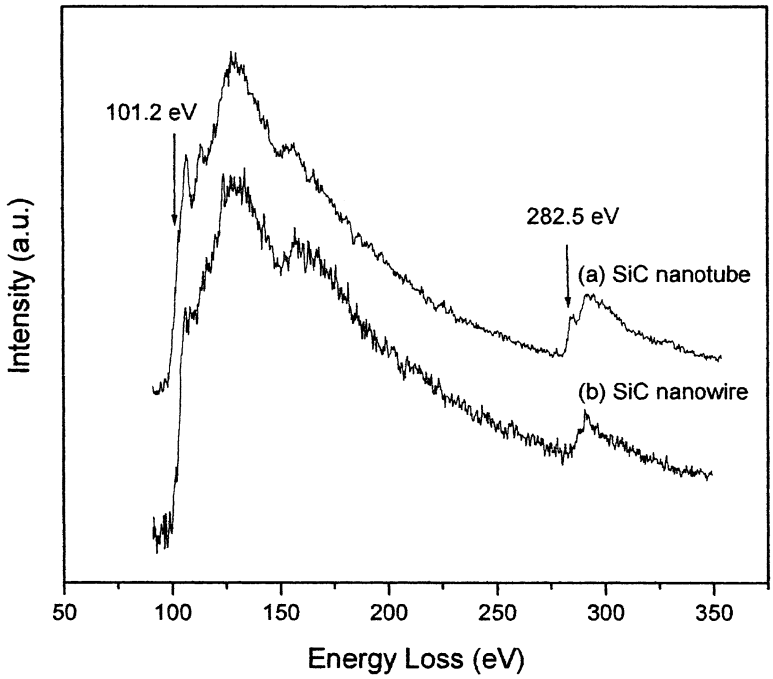

Fig. 18. EELS spectra of (a) a single SiC nanotube and (b) a single SiC nanowire. (Reprinted with permission from Ref. [45]. Copyright (2002) American Chemical Society.)

microtechnology. To date, prototype nanodevices such as transistors, diodes, switches, light-emitting diodes, lasers, chemical and biological sensors, etc. have been fabricated from SiNWs and SiNDs [32,106–111]. For example, dopants such as B and P can be introduced into SiNWs during synthesis making them p- or n-type semiconductors, respectively [31]. This can be done with different wires or within the same wire (segmented). Wiring these prototypes together to form logic gates, memories, and circuitries will build the foundation for future nanocomputer and other devices. Since some nanowires, including SiNWs, can also be made to emit light or to lase [111], it is conceivable that nanoelectronics will soon be integrated with nanophotonics [112].

Instead of building Si-based nanodevices "bottom-up" from individual SiNWs and SiNDs, it is also possible to fabricate Si nanodevices "top–down" by etching silicon chips. For nanometer resolution, it is necessary to use electron beam lithography. One example is the single-electron memory and single-electron transistor nanodevices fabricated by Tsutsumi et al. using an inorganic SiO_2 electron beam resist [113]. These single-electron devices [113–115] are possible due to the carrier confinement and/or Coulomb blockade effects exhibited by the very narrow SiNWs and/or very small SiNDs (15 nm wide SiNW channel and 5–10 nm isolated silicon islands in the work by Tsutsumi et al. [113]).

10. Conclusion and future prospects

Throughout this review, we discussed mainly doing chemistry on the surfaces of SiNWs. In reality, much of the same chemistry can also be performed on the surfaces of SiNDs, though the resulting products may have different morphologies and/or properties (e.g. optical properties, quantum-size effects, etc.).

To build a materials base for nanotechnology, one needs to control or manipulate the properties, sizes, and shapes of materials at the nanometer level. For example, just like electroless metal plating is a widely used technique in electronics industry in depositing metals onto semiconductor surfaces, making ohmic contacts, etc., one must also learn how to modify, to deposit different materials, or to grow metal films, on the surfaces of SiNWs. These are precisely the motives behind doing "platform chemistry" on the surfaces of SiNWs (see Section 5). The use of SiNWs as "templates" or "molds" in the synthesis of conventional CNTs or the new HCNTs (Section 6) is another example of control over nanomaterials syntheses. If we now reverse the roles of Si and C, i.e. depositing Si on CNTs (as "templates"), we obtained the SiCNTs along with other SiC nanowires (Section 8). The use of zeolites as quasi-templates afforded ultrafine SiNWs measuring about 3 nm in diameter (Section 7). The finest nanowires of about 1 nm in diameter contains only five or six silicon atoms, making them molecular wires. These molecular-sized wires will be useful in the construction of nano or molecular devices such as the single-electron transistors and memories mentioned above.

In addition to doing chemistry on the surfaces of SiNWs, one can also envision using SiNWs as connectors, bridges, conveyors, etc. in the fabrication of nano or molecular devices, or simple stringing together 1-D arrays of devices. For example, as we learn to control the growth and size of

PIM clusters [76,77] onto the surfaces of SiNWs, it may ultimately be possible to deposit and drive (with proper ohmic contacts) various prototype PIM-based molecular devices (such as motors, rotors, actuators, or simple gears and bearings) [76a,76d] on the surfaces of SiNWs in a 1-D array.

Acknowledgements

This paper is dedicated to the memory of Anna Tang Lee. Her appreciation of life never ceases to inspire me. Much of the works reviewed here were performed during a sabbatical leave in 2002 by the author at the Center of Super-Diamond and Advanced Films, the City University of Hong Kong. The author is particularly grateful for the kind hospitalities that Professors S.T. Lee, N.B. Wong, R.Q. Zhang, and their colleagues, especially Dr. X.H. Sun and C.P. Li, extended to him during his visit. Their important contributions in the collaborative works are acknowledged in Refs. [39–45].

References

[1] (a) K.E. Drexler, Nanosystems: Molecular Machinery, Manufacturing, and Computation, Wiley, New York, 1992;
(b) Sci. Am. 285 (2001), Special Issue on Nanotechnology.;
(c) P. Ball, Nature 406 (2000) 118.
[2] (a) I. Amato, Science 38 (1998) 114;
(b) J.W. Judy, Smart Mater. Struct. 10 (2001) 1115;
(c) H. Heinrich, G. Bauer, F. Kuchar (Eds.), Physics and Technology of Submicron Structures, Springer-Verlag, Berlin, Heidelberg, 1988.
[3] (a) R.W. Keyes, IBM J. Res. Dev. (1988) 24–28;
(b) H. Ahmed, K. Nakazoto, Microelect. Eng. 32 (1996) 297;
(c) D.A. Muller, T. Sorsch, S. Moccio, F.H. Baumann, K. Evans-Lutterodt, G. Timp, Nature 399 (1999) 758;
(d) R.F. Service, Science 293 (2001) 785.
[4] See, for example: (a) J.-M. Lehn, Supramolecular Chemistry: Concepts and Perspectives, VCH, Weinheim, 1995. (b) F. Vogtle, Supramolecular Chemistry. An Introduction, Wiley, Chichester, 1991. (c) D.B. Amabilino, J.F. Stoddart, Chem. Rev. 95 (1995) 2725. (d) G. Ungar, Y. Liu, X. Zeng, V. Percec, W.-D. Cho, Science, 299 (2003) 1208.
[5] S. Iijima, Nature 354 (1991) 56.
[6] J.W.G. Wildoer, L.C. Venema, A.G. Rinzler, R.E. Smalley, C. Dekker, Nature 391 (1998) 59.
[7] T.W. Odom, J.-L. Huang, P. Kim, C.M. Lieber, Nature 391 (1998) 62.
[8] J.-C. Charlier, P. Lambin, Phys. Rev. B 57 (1998) R15037.
[9] G. Zhou, W.H. Duan, B.L. Gu, Chem. Phys. Lett. 333 (2001) 344.
[10] N. Hamada, S.I. Sawada, A. Oshiyama, Phys. Rev. Lett. 68 (1992) 1579.
[11] R. Saito, G. Dresselhaus, M.S. Dresselhaus, Physical Properties of Carbon Nanotubes, Imperial College Press, London, 1998.
[12] S.M. Ouyang, J.-L. Huang, C.L. Cheung, C.M. Lieber, Science 292 (2001) 702.
[13] P.G. Collins, M.S. Arnold, P. Avouris, Science 292 (2001) 706.
[14] S. Iijima, C.J. Brabec, J. Chem. Phys. 104 (1996) 2089.
[15] A. Thess, R. Lee, P. Nikolaev, H.J. Dai, P. Petit, P. Robert, C.H. Xu, Y.H. Lee, S.G. Kim, A.G. Rinzler, D.T. Colbert, G.E. Scuseria, D. Tomanek, J.E. Fischer, R.E. Smalley, Science 273 (1996) 483.
[16] C. Journet, W.K. Maser, P. Bernier, A. Loiseau, M.L. DelaChapelle, S. Lefrant, P. Deniard, R. Lee, J.E. Fischer, Nature 388 (1997) 756.
[17] J.W. Mintmire, B.I. Dunlap, C.T. White, Phys. Rev. Lett. 68 (1992) 631.
[18] N. Hamada, S.I. Sawada, A. Oshiyama, Phys. Rev. Lett. 68 (1992) 1579.
[19] R. Saito, M. Fujita, G. Dresselhaus, M.S. Dresselhaus, Appl. Phys. Lett. 60 (1992) 2204.
[20] R. Saito, M. Fujita, G. Dresselhaus, M.S. Dresselhaus, Phys. Rev. B 46 (1992) 1804.
[21] R. Saito, M.G. Dresselhaus, M.S. Dresselhaus, Phys. Rev. B 61 (2000) 2981.
[22] Y.F. Zhang, Y.H. Tang, N. Wang, D.P. Yu, C.S. Lee, I. Bello, S.T. Lee, Appl. Phys. Lett. 72 (1998) 1835.
[23] (a) A.M. Morales, C.M. Lieber, Science 279 (1998) 208;
(b) X. Duan, C.M. Lieber, Adv. Mater. 12 (2000) 298.
[24] D.P. Yu, Z.G. Bai, Y. Ding, Q.L. Hang, H.Z. Zhang, J.J. Wang, Y.H. Zou, W. Qian, G.C. Xiong, H.T. Zhou, S.Q. Feng, Appl. Phys. Lett. 283 (1998) 3458.
[25] N. Wang, Y.H. Tang, Y.F. Zhang, D.P. Yu, C.S. Lee, I. Bello, S.T. Lee, Chem. Phys. Lett. 283 (1998) 368.
[26] W.S. Shi, H.Y. Peng, Y.F. Zheng, N. Wang, N.G. Shang, Z.W. Pan, C.S. Lee, S.T. Lee, Adv. Mater. 12 (2000) 1343.
[27] Y.H. Tang, Y.F. Zhang, N. Wang, C.S. Lee, X.D. Han, I. Bello, S.T. Lee, J. Appl. Phys. 85 (1999) 7981.
[28] F.C.K. Au, K.W. Wong, Y.H. Tang, Y.F. Zhang, I. Bello, S.T. Lee, Appl. Phys. Lett. 75 (1999) 1700.
[29] S.G. Volz, G. Chen, Appl. Phys. Lett. 75 (1999) 2056.
[30] S.T. Lee, N. Wang, Y.F. Zhang, Y.H. Tang, MRS Bull. (1999) 36.
[31] Y. Cui, X. Duan, J. Hu, C.M. Lieber, J. Phys. Chem. B 104 (2000) 5213.
[32] Y. Cui, C.M. Lieber, Science 291 (2001) 851–853.
[33] Y.F. Zhang, L.S. Liao, W.H. Chan, S.T. Lee, R. Sammynaiken, T.K. Sham, Phys. Rev. B 61 (2000) 8296.
[34] X.H. Sun, H.Y. Peng, Y.H. Tang, W.S. Shi, N.B. Wong, C.S. Lee, S.T. Lee, T.K. Sham, J. Appl. Phys. 89 (2000) 6396.
[35] X.H. Sun, R. Sammynaiken, S.J. Naftel, Y.H. Tang, P. Zhang, P.S. Kim, T.K. Sham, X.H. Fan, Y.F. Zhang, N.B. Wong, C.S. Lee, S.T. Lee, Chem. Mater. 14 (2002) 2519.
[36] D.D.D. Ma, C.S. Lee, F.C.K. Au, S.Y. Tong, S.T. Lee, Science 299 (2003) (1874) 1877.
[37] X.H. Sun, N.B. Wong, S.T. Lee, B.K. Teo, to be published.
[38] B. Marsen, K. Sattler, Phys. Rev. B 60 (1999) 11593.
[39] R.Q. Zhang, S.T. Lee, C.K. Law, W.K. Li, B.K. Teo, Chem. Phys. Lett. 364 (2002) 251.
[40] X.H. Sun, S.D. Wang, N.B. Wong, D.D.D. Ma, S.T. Lee, B.K. Teo, Inorg. Chem. 42 (2003) 2398.
[41] X.H. Sun, C.P. Li, N.B. Wong, C.S. Lee, S.T. Lee, B.K. Teo, Inorg. Chem. 41 (2002) 4331.
[42] C.P. Li, X.H. Sun, N.B. Wong, C.S. Lee, S.T. Lee, B.K. Teo, J. Phys. Chem. B 106 (2002) 6980.
[43] X.H. Sun, C.P. Li, N.B. Wong, C.S. Lee, S.T. Lee, B.K. Teo, J. Am. Chem. Soc. 124 (2002) 14856.
[44] C.P. Li, X.H. Sun, N.B. Wong, C.S. Lee, S.T. Lee, B.K. Teo, Chem. Phys. Lett. 365 (2002) 22.
[45] X.H. Sun, C.P. Li, W.K. Wong, N.B. Wong, C.S. Lee, S.T. Lee, B.K. Teo, J. Am. Chem. Soc. 124 (2002) 14464.
[46] S.B. Fagan, R.J. Barierle, R. Mota, A.J.R. da Silva, A. Fazzio, Phys. Rev. B 61 (2000) 9994.
[47] G. Seifert, T. Köhler, H.M. Urbassek, E. Hernández, T. Frauenheim, Phys. Rev. B 63 (2001) 193409.
[48] J.W. Kang, J.J. Seo, H.J. Hwang, J. Nanosci. Nanotech. 2 (2002) 687.
[49] J. Sha, J. Niu, X. Ma, J. Xu, X. Zhang, Q. Yang, D. Yang, Adv. Mater. 14 (2002) 1219.
[50] B.K. Teo, C.P. Li, X.H. Sun, N.B. Wong, S.T. Lee, Inorg. Chem. 42 (2003) 6723.
[51] H.Y. Peng, N. Wang, Y.F. Zhang, Y. Lifshitz, J. Kulik, R.Q. Zhang, C.S. Lee, S.T. Lee, Appl. Phys. Lett. 77 (2000) 2831.

[52] L.C. Qin, X. Zhao, K. Hirahara, Y. Miyamoto, Y. Ando, S. Iijima, Nature 408 (2000) 50.
[53] N. Wang, Z.K. Tang, G.D. Li, J.S. Li, Nature 408 (2000) 50.
[54] J.J.P. Stewart, J. Comput. Chem. 2 (1989) 209.
[55] M.J.S. Dewar, W.J. Thiel, J. Am. Chem. Soc. 99 (1977) 4899.
[56] Q. Liu, S.M. Kauzlarich, Mater. Sci. Eng. B 96 (2002) 72.
[57] T. Unagami, M. Seki, J. Electrochem. 125 (1978) 1339.
[58] Y. Kato, T. Ito, A. Hiraki, Jpn. J. Appl. Phys. 27 (1988) L1406.
[59] M. Grundner, H. Jakob, Appl. Phys. A 39 (1986) 73.
[60] D. Gräf, M. Grundner, R.J. Schulz, Appl. Phys. 68 (1990) 155.
[61] V.A. Burrows, Y.J. Chabal, G.S. Higashi, K. Raghavachari, S.B. Christman, Appl. Phys. Lett. 53 (1988) 998.
[62] G.S. Higashi, Y.J. Chabal, G.W. Trucks, K. Raghavachari, Appl. Phys. Lett. 56 (1990) 656.
[63] Y.J. Chabal, G.S. Higashi, K. Raghavachari, V.A. Burrows, J. Vac. Sci. Technol. A 7 (1989) 2104.
[64] P. Jakob, Y.J. Chabal, J. Chem. Phys. 95 (1991) 2897.
[65] M.A. Hines, Y.J. Chabal, T.D. Harris, A.L. Harris, Phys. Rev. Lett. 71 (1993) 2280.
[66] M. Niwano, M. Terash, M. Shinohara, D. Shoji, N. Miyamoto, Surf. Sci. 401 (1998) 364.
[67] M. Niwano, J. Kageyama, K. Kinashi, J. Sawahata, N. Miyamoto, Surf. Sci. 301 (1994) 245.
[68] K. Sugiyama, T. Igaraschi, K. Moriki, Y. Nagasawa, T. Aoyama, R. Sugino, T. Ito, T. Hattori, Jpn. J. Appl. Phys. 29 (1990) L2401.
[69] H. Ogawa, K. Ishikawa, M.T. Suzuki, Y. Hayami, S. Fujimura, Surf. Sci. Lett. 302 (1993) 245.
[70] Y. Sugita, S. Watanabe, Jpn. J. Appl. Phys. 37 (1998) 1193.
[71] M.L.W. van der Zwan, J.A. Bardwell, G.I. Sproule, M.J. Graham, Appl. Phys. Lett. 64 (1994) 446.
[72] D.R. Bowler, J.G. Owen, K. Miki, G.A.D. Briggs, Phys. Rev. B 57 (1998) 8790.
[73] R. Houberts, U. Memmert, R.J. Behm, Surf. Sci. 396 (1998) 198.
[74] G. Hollinger, F.J. Himpsel, J. Vac. Sci. Technol. A 1 (1983) 640.
[75] P.O. Hahn, Mater. Res. Soc. Symp. Proc. 54 (1986) 645.
[76] (a) B.K. Teo, H. Zhang, Coord. Chem. Rev. 143 (1995) 609;
(b) H. Zhang, B.K. Teo, Inorg. Chim. Acta 265 (1997) 213;
(c) B.K. Teo, H. Zhang, Inorg. Chim. Acta 317 (2001) 1;
(d) B.K. Teo, H. Zhang, Angew. Chem. Int. Ed. Engl. 31 (1992) 445.
[77] (a) B.K. Teo, H. Dang, C. Campana, H. Zhang, Polyhedron 17 (1998) 617;
(b) B.K. Teo, H. Zhang, J. Organanomet. Chem. 614–615 (2000) 66;
(c) B.K. Teo, H. Zhang, X. Shi, Inorg. Chem. 33 (1994) 4086;
(d) B.K. Teo, H. Zhang, J. Cluster Sci. 12 (2001) 357.
[78] L.D. Marks, M.C. Hong, H. Zhang, B.K. Teo, Mater. Res. Soc. Symp. Proc. 111 (1989) 213.
[79] P.M. Ajayan, L.D. Marks, Nature 338 (1989) 139.
[80] S. Iijima, T. Ichihashi, Phys. Rev. Lett. 56 (1986) 616.
[81] D.J. Smith, A.K. Petford-Long, L.R. Wallenberg, J.O. Bovin, Science 233 (1986) 872.
[82] P.M. Ajayan, L.D. Marks, Phys. Rev. Lett. 56 (1988) 585.
[83] N. Doraiswamy, L.D. Marks, Surf. Sci. 384 (1996) 67.
[84] A. Howie, Nature 320 (1986) 684.
[85] M. Zinke-Allmang, L.C. Feldman, S. Nakahara, Appl. Phys. Lett. 51 (1987) 975.
[86] R.S. Wagner, W.C. Ellis, Appl. Phys. Lett. 4 (1964) 89.
[87] N. Wang, Y.H. Tang, Y.F. Zhang, C.S. Lee, S.T. Lee, Chem. Phys. Lett. 299 (1999) 237.
[88] S.T. Lee, Y.F. Zhang, N. Wang, Y.H. Tang, I. Bello, C.S. Lee, Y.W. Chung, J. Mater. Res. 12 (1999) 4503.
[89] C.P. Li, N. Wang, S.P. Wong, C.S. Lee, S.T. Lee, Adv. Mater. 14 (2002) 218.
[90] S. Iijima, T. Ichihashi, Nature 363 (1993) 603.
[91] D. Ugarte, Nature 359 (1992) 707.
[92] T.W. Ebbesen, P.M. Ajayan, Nature 358 (1992) 220.
[93] J. Kong, A.M. Cassell, H.J. Dai, Chem. Phys. Lett. 292 (1998) 567.
[94] W.A. De Heer, D. Ugarte, Chem. Phys. Lett. 207 (1993) 480.
[95] Y.L. Hsin, K.C. Hwang, F.R. Chen, J.J. Kai, Adv. Mater. 13 (2001) 830.
[96] N. Sano, H. Wang, M. Chhowalla, I. Alexandrou, G.A.J. Amaratunga, Nature 414 (2001) 505.
[97] Previous work by H. Nishihara, H. Harada, M. Tateishi, K. Ohashi, K. Aramaki, J. Chem. Soc. Farad. Trans. 87 (1991) 1187, showed that electrochemical reduction of halogenated organic compounds can lead to carbonaceous or graphitic deposits. These electrodeposited materials typically have a molecular structure resembling turbostratic graphite.
[98] H.J. Dai, E.W. Wong, Y.Z. Lu, S.S. Fan, C.M. Lieber, Nature 375 (1995) 769.
[99] Z. Pan, H.L. Lai, F.C.K. Au, X.F. Duan, W.Y. Zhou, W.S. Shi, N. Wong, C.S. Lee, N.B. Wong, S.T. Lee, Adv. Mater. 12 (2000) 1186.
[100] W.Q. Han, S.S. Fan, Q.Q. Li, Y.D. Hu, Science 277 (1997) 1287.
[101] Y. Zhang, K. Suenaga, C. Colliex, S. Iijima, Science 281 (1998) 973.
[102] Y. Zhang, T. Ichihashi, E. Landree, F. Nihey, S. Iijima, Science 285 (1999) 1719.
[103] Z.L. Wang, Z.R. Dai, R.P. Gao, Z.G. Bai, J.L. Gole, Appl. Phys. Lett. 77 (2000) 3349.
[104] G.L. Harris (Ed.) Properties of Silicon Carbide, INSPEC, Institution of Electrical Engineers, London, 1995.
[105] L. Moro, A. Paul, D.C. Lorents, R. Malhotra, R.S. Ruoff, P. Lazzeri, L. Vanzetti, A. Lui, S. Subramoney, J. Appl. Phys. 81 (1997) 6141.
[106] (a) P.M. Ajayan, O.Z. Zhou, Top. Appl. Phys. 80 (2001) 391;
(b) P. Ball, Nature 414 (2001) 142.
[107] Y. Huang, X. Duan, Y. Cui, C.M. Lieber, Nano Lett. 2 (2002) 101.
[108] F. Kim, S. Kwan, J. Akana, P. Yang, J. Am. Chem. Soc. 123 (2001) 4360.
[109] X. Duan, Y. Huang, C.M. Lieber, Nano Lett. 2 (2002) 487.
[110] Y. Cui, Q. Wei, H. Park, C.M. Lieber, Science 293 (2001) 1289.
[111] L. Pavesi, L. Dal Negro, G. Mazzoleni, G. Franzo, F. Priolo, Nature 408 (2000) 440.
[112] M.H. Huang, S. Mao, H. Feick, H. Yan, Y. Wu, H. Kind, E. Weber, R. Russo, P. Yang, Science 292 (2001) 1897.
[113] T. Tsutsumi, E. Suzuki, K. Ishii, H. Hiroshima, M. Yamanaka, I. Sakata, S. Hazra, K. Tomizawa, Superlatt. Microstruct. 28 (2000) 453.
[114] M.A. Kastner, Rev. Mod. Phys. 64 (1992) 849.
[115] E. Leobandung, L. Guo, Y. Wang, S.Y. Chou, Appl. Phys. Lett. 67 (1995) 938.